ELSEVIER

Physics of the Earth and Planetary Interiors 88 (1995) 117–130

PHYSICS OF THE EARTH AND PLANETARY INTERIORS

On seismic resolution of lateral heterogeneity in the Earth's outermost core

Edward J. Garnero *, Donald V. Helmberger

California Institute of Technology, Seismological Laboratory 252-21, Pasadena, CA 91125, USA

Received 3 February 1994; revision accepted 19 July 1994

Abstract

Issues concerning resolution of seismically determined outermost core properties are presented with an example from three earthquakes in the Fiji–Tonga region. Travel time behavior of the commonly used family of SmKS waves, which travel as S in the mantle, P in the core, reflecting $m-1$ times at the underside of the core–mantle boundary (CMB), are analyzed over a large distance range (125–165°). Data having wavepaths through an area of known D″ heterogeneity (±2%) exhibit systematic anomalies in SmKS differential times. Two-dimensional wave propagation experiments demonstrate how large-scale lower-mantle velocity perturbations can explain long-wavelength behavior of such anomalous SmKS times, though heterogeneity on smaller scales may be responsible for the observed scatter about these trends. If lower-mantle heterogeneity is not properly accounted for in deriving a core model, misfit of the mantle model maps directly into core structure. The existence of outermost core heterogeneity is difficult to resolve at present, owing to uncertainties in global lower-mantle structure. Resolving a one-dimensional chemically stratified outermost core also remains difficult, owing to the same uncertainties. Inclusion of the slowly accruing broadband data should help in this regard. Restricting study to higher multiples of SmKS ($m = 2, 3, 4$) can help reduce the effect of mantle heterogeneity, because of the closeness of the mantle legs of the wavepaths. SmKS waves are ideal in providing additional information on the details of lower-mantle heterogeneity.

1. Introduction

The structure and dynamics of Earth's outer core play an increasingly important role in multidisciplinary studies of the region. In particular, whether or not the outermost core contains lateral heterogeneity or chemical stratification will have strong implications on fluid motions and patterns immediately beneath the core–mantle boundary (CMB) and hence the geomagnetic field, as well as the overall dynamical, chemical and thermomechanical behavior. As progress is made in theoretical studies of such physical properties (e.g. Fearn and Loper, 1981; Bloxham, 1990; Jault and Le Mouël, 1991), parallel progress in resolving these phenomena in the Earth is desired. At present, to detect lateral heterogeneity and chemical stratification in the Earth's outermost core, seismic remote sensing methods must be employed. However, as the seismic approach is an indirect way of getting at these issues, inherent uncertainties exist. It is the focus of this

* Corresponding author at: Institute of Tectonics, University of California, Santa Cruz, CA 95064, USA.

SSDI 0031-9201(94)02976-8

work to analyze seismic data commonly used for such study, and to present the resolution and uncertainties of these data.

The only documented commonly recorded seismic phases with wavepath turning depths in the topmost half of the outer core are the family of SmKS waves ($m = 1$–4). These phases travel as SV waves in the mantle, convert to P waves in the core, reflecting $m - 1$ times at the underside of the CMB, then convert back to SV for the final mantle leg of the path. SmKS are the outermost core's equivalent to upper-mantle multi-reflected S waves, S, SS, SSS, etc., and provide a dense sampling of the outer core over an extended distance range (85–165° and beyond). Commonly notated as SKS, SKKS, SKKKS, etc., we use the notation SKS, S2KS, S3KS, etc., to denote the separate phases. A shorthand is used to designate specific SmKS by writing the values of m as a subscript; for example, $SmKS_{234}$ indicates SmKS with $m = 2, 3, 4$, or S2KS, S3KS, and S4KS, respectively. If no subscript is written then we are referring to any value of m. SmKS waves having ray turning depths near the top of the outer core are possibly the best suited seismic waves for providing information on outermost core heterogeneity, chemical stratification, and general one-dimensional (1-D) structure, and for this reason have been prolifically used in outer-core modeling studies.

Previous seismic studies investigating 1-D outermost core structure have relied upon SKS times (e.g. Randall, 1970), $SmKS_{12}$ times (e.g. Hales and Roberts, 1971; Schweitzer and Muller, 1986; Lay and Young, 1990; Tanaka and Hamaguchi, 1993a), $SmKS_{123}$ times (Souriau and Poupinet, 1991), and $SmKS_{234}$ (Garnero et al., 1993a). Studies presenting globally averaged 1-D reference Earth models have used a combination of $SmKS_{12}$ times and normal mode periods (e.g. Dziewonski and Anderson, 1981; Kennett and Engdahl, 1991; Morelli and Dziewonski, 1993). SmKS has also been used to infer outermost core heterogeneity (e.g. Schweitzer, 1990; Souriau and Poupinet, 1990; Kohler and Tanimoto, 1992; Tanaka and Hamaguchi, 1993b) and chemical stratification at the top of the core (e.g. Lay and Young, 1990; Garnero et al., 1993a; Tanaka and Hamaguchi, 1993c). Chemical and thermal stratification can also be pursued from observations of the periods of normal modes, though resolution at vertical scales smaller than 200 km for this method is difficult (see Masters (1979) for a thorough treatment of this approach and discussion of uncertainties involved). Some studies have incorporated modeling of lower-mantle heterogeneity in explaining anomalous $SmKS_{12}$ times (e.g. Garnero et al., 1988; Schweitzer, 1990) or removed the effects of previously published aspherical mantle models (e.g. Schweitzer, 1990; Tanaka and Hamaguchi, 1993abc). Many of the above studies have utilized differential rather than absolute times of SmKS in an effort to minimize the effect of mantle heterogeneity. How mantle heterogeneity may affect the various SmKS phases is explored in detail in this study.

Of particular relevance in outer-core modeling using SmKS are the scale lengths of the distances between wavepaths of adjacent SmKS waves (Garnero et al., 1993a). $SmKS_{12}$ for the commonly studied distance range (100–130°) have raypaths separated by around 700 km at the CMB crossing locations (on the source or receiver side of paths). Any mantle heterogeneity having scale lengths of this order or smaller will thus affect such times. Whereas tomographic inversions for global maps of V_S structure typically have minimum lower-mantle resolution of scale length $O(1000)$ km (e.g. Tanimoto, 1990; Masters et al., 1992; Su et al., 1992), body-wave analyses have provided evidence for large changes in lower-mantle V_S over shorter scale lengths of $O(100)$ km (e.g. Lavely et al., 1986; Garnero et al., 1988; Schweitzer, 1990; Weber and Davis, 1990; Gaherty and Lay, 1992; Weber, 1993; Bokelmann and Silver, 1993; Wysession et al., 1994). The CMB separation of higher-multiple SmKS raypaths is even smaller: around 200–300 km for $SmKS_{23}$ separation, and 100–150 km for $SmKS_{34}$ (Garnero et al., 1993a). These higher multiples have not been used in past studies for core structure, probably owing to the abundance of unanalyzed $SmKS_{12}$ data. Tanaka and Hamaguchi (1993a), however, did analyze $SmKS_{23}$ difference time behavior, but did not include it in their modeling procedure.

In what follows, we present our method of generating 1- and 2-D synthetic seismograms for comparison with observations. Scale lengths of resolution for the data, uncertainties in the model space, and the importance of laterally inhomogeneous raypaths are then discussed, with an example from a set of three earthquakes in the Fiji–Tonga region.

2. Synthetic seismograms

The reflectivity method (see, e.g. Fuchs and Müller, 1971; Müller, 1985) is used as a 1-D reference technique for computing synthetic seismograms. We also utilize a modified WKBJ technique for computation of 1- and 2-D synthetics. The modified WKBJ method, denoted WKM, was discussed by Helmberger et al. (1995), but their analysis does not extend to the large epicentral ranges studied here. Hence some additional issues not presented by Helmberger et al. (1995) relating to WKM generation of large distance S*m*KS are discussed below.

As indicated by Chapman and Orcutt (1985), WKBJ seismograms compare well with reflectivity except for regions containing interference of S*m*KS-coupled head waves generated along the CMB. These waves, denoted as SP_dKS, have been described by Choy (1977) and pointed out in reflectivity synthetics by Kind and Müller (1975). Observations of SP_dKS relative to SKS have been analyzed by Garnero et al. (1993b).

SP_dKS waves are generated at the ray parameter associated with the critical angle for ScP waves incident on the CMB. This ray parameter corresponds to SKS waves at around 107° (which is a model-dependent distance). Amplitudes of SKS at this ray parameter diminish owing to the loss of energy that goes into creating SP_dKS (Silver and Bina, 1993), and at infinite frequency the SKS transmission coefficient goes to zero. S2KS, S3KS, and S4KS energies at this same ray parameter are affected similarly. The WKBJ method does not properly account for this diffraction effect associated with SP_dKS. It does, however, include the correct CMB transmission coefficients that go to zero at the ScP critical angle.

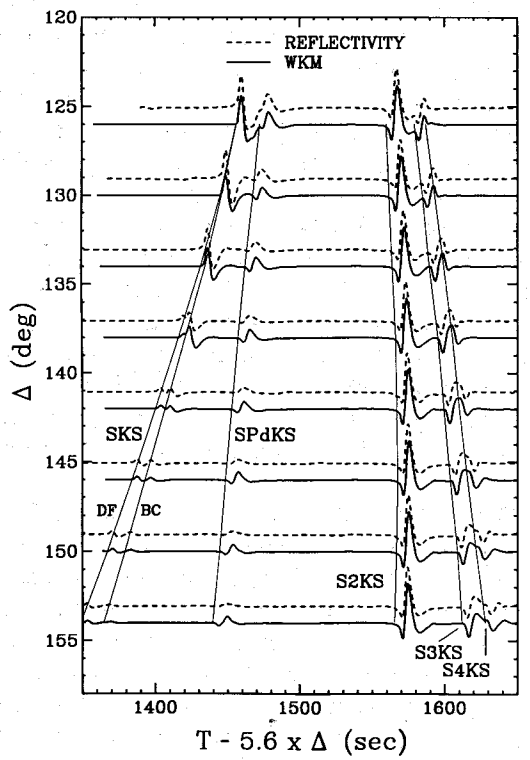

Fig. 1. LP WWSSN WKM (solid) and reflectivity (dotted) synthetics compared for the PREM. Travel time curves are for WKM traces, for which the reflectivity traces are plotted above.

The zero in transmission coefficients generates a truncation arrival in each SmKS arrival, and causes undesirable interference in the $SmKS_{234}$ wave packet. We circumvent this by imposing a 'water level' for the transmission coefficients at a ray parameter slightly before the critical angle ray parameter where the transmission coefficient vanishes. This in turn produces synthetics that match extremely well with reflectivity seismograms (Fig. 1) for the Preliminary Reference Earth Model (PREM; Dziewonski and Anderson, 1981). The profile displayed is for a source depth of 500 km, and responses are filtered through a long-period (LP) World-Wide Seismographic Station Network (WWSSN) instrument. For every bounce off the underside of the CMB, S*m*KS experiences a $\pi/2$ phase shift (a Hilbert transform; see Choy and Richards (1975) and Choy

(1977)), which is included in both techniques. Agreement between WKM and reflectivity at smaller distances is also excellent (Helmberger et al., 1995).

The water-level approximation remains valid as the first arrival energy of $SmKS_{234}$ arrives significantly earlier in time than the energy associated with the critical angle ray parameter. However, this is not the case with SKS, as SKS first arrival energy arrives close in time to SP_dKS. For this reason, we did not modify SKS transmission coefficients, and expect some misfit of the WKM SP_dKS arrival, especially at distances around 110°. Nonetheless, SKS travel time behavior at this distance can still be analyzed, as will be shown below.

The WKM method can accommodate 2-D velocity structures containing iso-velocity layers that can vary in thickness in any manner, as long as raypaths do not bottom in laterally varying structure, which is avoided here as the core is kept 1-D in these experiments. Models containing various dipping structures, or low- or high-velocity cosine tapers in D″, for example, can thus be explored without the assumption of lateral homogeneity in the raypath. This method is applied to SmKS with respect to examples of WWSSN data exhibiting travel time anomalies. The following section presents a sample of data, which is followed by some preliminary modeling experiments.

3. Data set and travel times

Because of the long time-span of continuous operation, abundant SmKS data from the WWSSN archives are available (around two decades of deep focus events recorded worldwide.) SmKS data are well recorded over a large distance range (85° to beyond 165°) on the LP channel with periods of 10–20 s. Deep focus events are used to minimize any possible slab effects (Cormier, 1989), source-side complexities and interference from surface reflected phases.

Only SmKS ($m = 2, 3, 4$) data are presented here, in an effort to minimize effects of mantle heterogeneity, as the difference in their mantle paths is significantly smaller than the difference between SKS and SKKS. SKKS–SKS times, $T_{S2KS-SKS}$ (and, to a greater content, S–SKS times, T_{S-SKS}), can be significantly affected by mantle structure (Garnero et al., 1988; Schweitzer, 1990; Garnero and Helmberger, 1993). For example, deep focus Fiji–Tonga events display $T_{S2KS-SKS}$ times up to 5 s greater than that predicted by the PREM. This same region was shown to exhibit T_{S-SKS} times up to 10 s greater than PREM predictions; and when correcting these times for various aspherical structures presented in the literature, up to 4 s anomalies remain for T_{S-SKS} times (Garnero and Helmberger, 1993). This point is made to emphasize that unmapped mantle structure on many different scale lengths contribute to observed travel time perturbations in $SmKS_{12}$. Schweitzer (1990) emphasized that smooth long-wavelength aspherical structures could not predict $T_{S2KS-SKS}$ anomalies for the Fiji–Tonga data, and concluded that mantle structure surely contributes to $T_{S2KS-SKS}$ observations. Moving to higher-multiple SmKS waves results in the following: (1) the bottoming depths of raypaths in the outer core are significantly closer to the CMB, thus improving coverage in the outermost few hundred kilometers of the core; (2) effects of mantle heterogeneity are reduced (Souriau and Poupinet, 1990; Garnero et al., 1993a); (3) an extended distance range is allowed, much beyond the limits of $T_{S2KS-SKS}$ (which is limited by SKS amplitudes dying out near 130°). Thus the effective distance range for studying $SmKS_{234}$ is 125–165° and beyond.

Fiji–Tonga sources recorded in Eurasia and Africa provide an opportunity to study $SmKS_{234}$ out to 165° because of the station geometry. Fig. 2 presents great circle raypaths for three deep focus Tonga events. The circles denote the CMB crossing locations of $SmKS_{234}$ and the triangles are WWSSN stations. The optically scanned, digitized and rotated data are displayed in Fig. 3, with the S2KS arrivals aligned in time and normalized in amplitude. The dotted lines depict the observed arrivals of $SmKS_{234}$. Most of the data are cleanly recorded, although, as we will demonstrate, travel time anomalies exist. $T_{S3KS-S2KS}$ and

$T_{S4KS-S3KS}$ times for the data and the PREM were measured through the cross-correlation method. For all observations, S2KS was Hilbert transformed to be in phase with S3KS, and S3KS was Hilbert transformed to be in phase with S4KS, before the correlation scheme. The resulting difference times were double checked by overlaying records with synthetics of appropriate distance, source depth, and source time function.

Residual $T_{S3KS-S2KS}$ and $T_{S4KS-S3KS}$ times ($\delta T_{S3KS-S2KS}$ and $\delta T_{S4KS-S3KS}$, respectively) of the Tonga events are plotted in Fig. 4 as a function of epicentral distance and source azimuth. A ± 1 s error bar is included to emphasize that some error may be induced through the digitization procedure, as well as from the correlation procedure when the signal-to-noise ratio (SNR) is low. Phase misidentification can lead to even larger errors, although $SmKS_{234}$ are generally easily identified, or the records are not included in our analysis. $\delta T_{S3KS-S2KS}$ and $\delta T_{S4KS-S3KS}$ times plotted with distance (Figs. 4(a) and 4(b)) display large scatter, with most observations exhibiting S3KS–S2KS and S4KS–S3KS separations larger than PREM predictions. However, when viewed in terms of source azimuth, the angle between north and the great circle source–receiver path (measured clockwise), some systematics appear

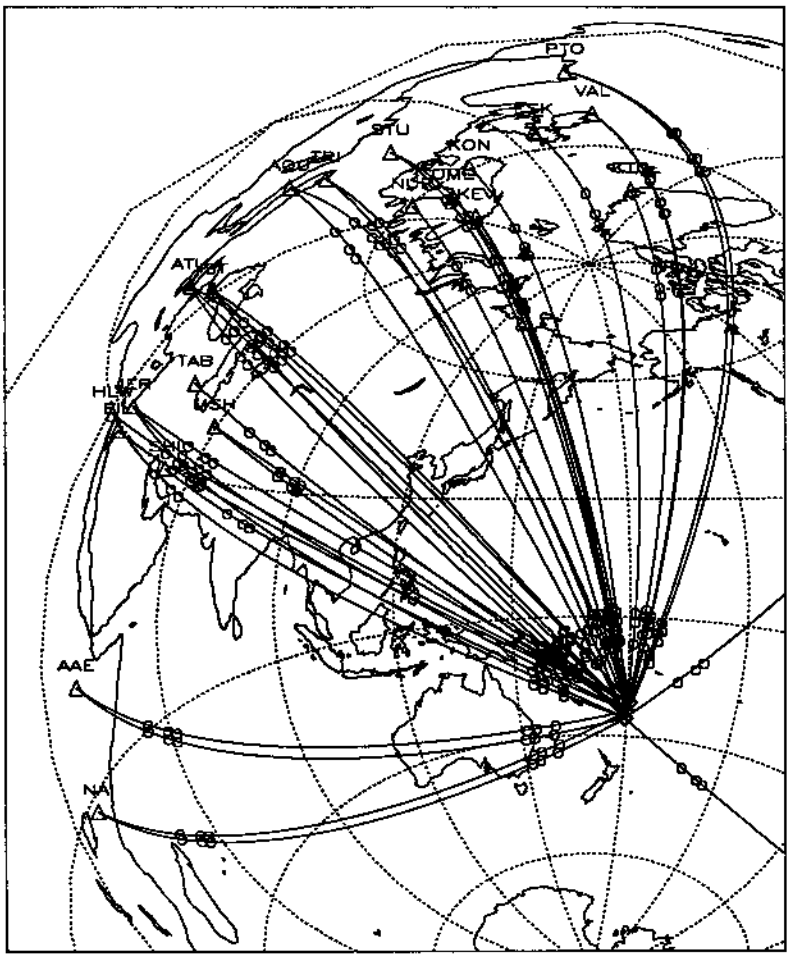

Fig. 2. Great circle raypaths for three Tonga events recorded in Eurasia and Africa. Open circles denote $SmKS_{234}$ CMB crossing locations projected to the Earth's surface.

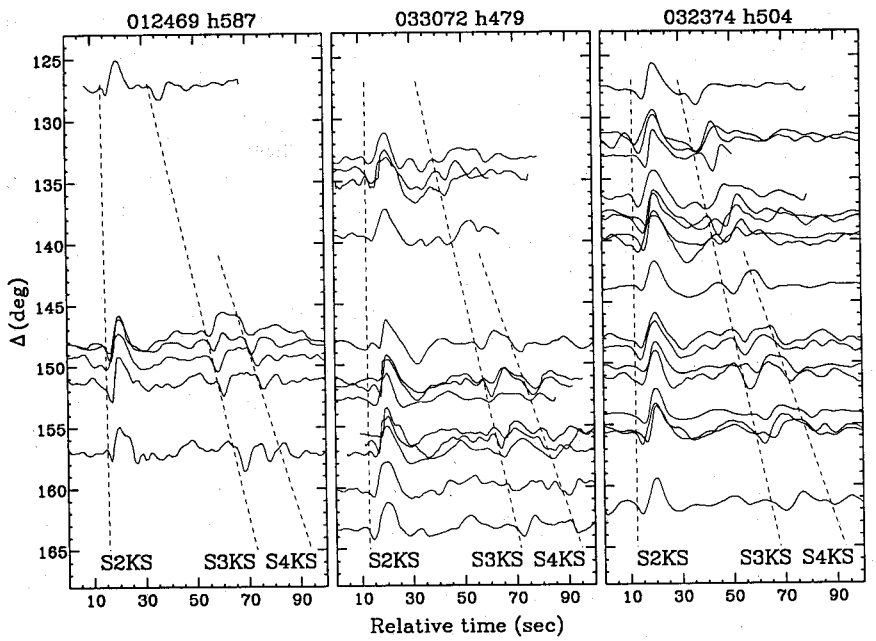

Fig. 3. LP WWSSN profiles for three deep focus Tonga events. Dotted lines correspond to observed arrival times of $SmKS_{234}$.

(Fig. 4(c) and 4(d)). Each datum is plotted at the azimuth to its respective source; the three Tonga sources are located closely enough for this not to induce any errors of significance in viewing all three events on the same plot. For azimuths between 280 and 350°, $\delta T_{S3KS-S2KS}$ times are

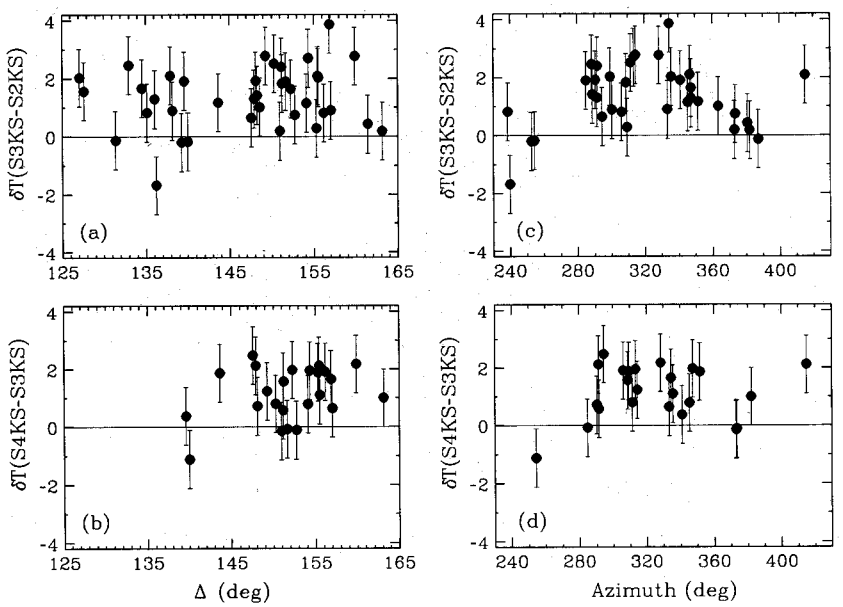

Fig. 4. (a) $\delta T_{S3KS-S2KS}$ and (b) $\delta T_{S4KS-S3KS}$ residuals as a function of distance, and (c) $\delta T_{S3KS-S2KS}$ and (d) $\delta T_{S4KS-S3KS}$ residuals plotted against azimuth from source. All residuals are observed minus PREM predictions.

systematically delayed by up to several seconds with respect to the PREM (Fig. 4(c)). The data outside this azimuth window, though sparse, taper to values around the PREM prediction (with a few exceptions). The long-wavelength trend of the $\delta T_{S3KS-S2KS}$ times vs. azimuth resembles a concave-down curve, and is explored below. The set of $\delta T_{S4KS-S3KS}$ times in Fig. 4 is smaller than that of $\delta T_{S3KS-S2KS}$ times, owing to the fact that S4KS cannot be reliably measured until almost 140° in distance. The fewer points in Fig. 4(d) make identification of any particular trend difficult. Nonetheless, the $\delta T_{S4KS-S3KS}$ points seem to fall within the scatter and trend of Fig. 4(c).

In analyzing such trends in SmKS times, the inherent trade-off between mantle and core structure is ever present. Although we are not currently in a position to resolve this ambiguity, we can investigate effects of mantle structure on SmKS times. The source-side $SmKS_{234}$ lower-mantle wavepaths for the Fiji–Tonga events (Fig. 2) traverse anomalously slow and laterally varying V_S structure, as suggested by both body-wave (e.g. Woodward and Masters, 1991; Wysession et al., 1992, 1994) and global tomographic inversion studies (e.g. Masters et al., 1992; Su et al., 1992). For the remainder of this paper, the aspherical structure of Su et al. (1992), SH12_WM13, is used in discussions of lower-mantle V_S lateral variations. This model is nearly identical to the recently updated version presented by Su et al. (1994). This choice of model is somewhat arbitrary, as other 3-D models will lead to similar conclusions that follow.

The map view of the D″ layer V_S perturbations (δV_S) for SH12_WM13 is presented in Fig. 5, along with the S2KS (crosses) and S3KS (circles) CMB crossing locations, and the Tonga sources (stars). As a first step, δV_S from SH12_WM13 has been extracted for the D″ layer for the corresponding locations of the S2KS and S3KS CMB crossing locations for the Tonga data. The SH12_WM13 δV_S values for both the source and receiver sides of the Tonga wavepaths are displayed in Fig. 6(a) with respect to azimuth from source, as in Figs. 4(c) and 4(d). The solid and open crosses designate δV_S at the receiver-side S2KS and S3KS CMB crossing locations, respectively. The solid and open triangles designate δV_S at the source-side S2KS and S3KS CMB crossing

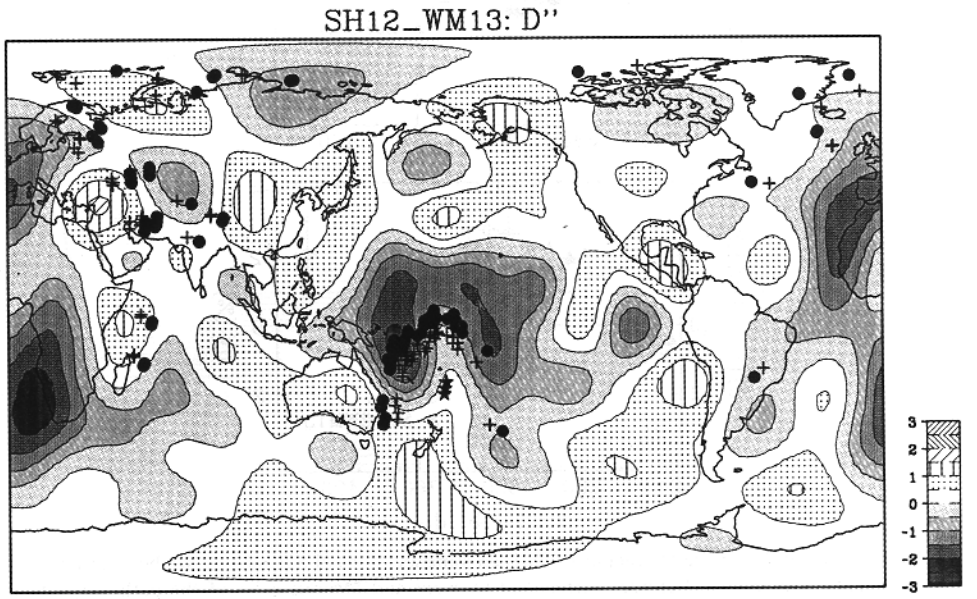

Fig. 5. Aspherical structure of D″ as depicted by SH12_WM13, along with S2KS (crosses) and S3KS (circles) CMB crossing locations for the Tonga sources (stars). Dark regions are slower than average and white regions are faster than average.

locations, respectively. The vertical axis plotting convention is such that negative δV_S values are plotted above the zero line, which corresponds to slower than average V_S regions; conversely, values below the zero line correspond to faster than average velocities. As the figure illustrates, receiver-side D″ predictions from SH12_WM13 are roughly within $\pm 1\%$, whereas source-side perturbations display an azimuthal trend with pronounced slow velocities (more than 2% slower than average) near 300° in azimuth from the Tonga source region.

Fig. 6(b) displays the average of the source-side δV_S values of Fig. 6(a), along with averaged $\delta T_{S3KS-S2KS}$ times of Fig. 4(c). The $\delta T_{S3KS-S2KS}$ times and δV_S perturbations were averaged in 10° azimuth bins. The vertical axes for δV_S and $\delta T_{S3KS-S2KS}$ values are on the right and left sides of the figure, respectively. Only the source-side δV_S values are included, as the receiver-side values are small on average throughout the azimuth range. Also, the δV_S values for the S2KS and S3KS CMB crossing locations have been averaged in Fig. 6(b). The azimuthal trend of SH12_WM13 δV_S values predicts slower than average V_S values in locations where $\delta T_{S3KS-S2KS}$ observations display anomalously large S3KS–S2KS time separations. Fig. 6(b) suggests qualitative agreement between SH12_WM13 and the $\delta T_{S3KS-S2KS}$ residuals. This model is used as a starting point in our modeling experiments below, in which we investigate the effects of laterally varying structure on the travel times of $SmKS_{234}$.

4. 2-D modeling experiments

The effects of lower mantle laterally varying structure on synthetic $SmKS_{234}$ waveforms are explored in this section. In the 1-D sense, slower

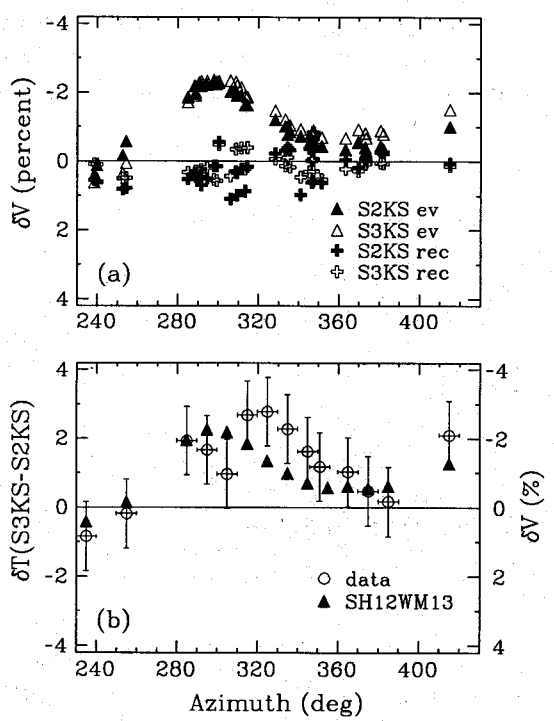

Fig. 6. (a) SH12_WM13 δV_S values for the D″ region at CMB crossing locations of S2KS (solid symbols) and S3KS (open symbols) for the three Tonga events. Triangles and crosses correspond to event and receiver sides of the path, respectively. (b) The 10° azimuth bin averages of SH12_WM13 δV_S perturbations for the Tonga source-side $SmKS_{23}$ CMB crossing points (triangles, vertical scale on right) and the observed $\delta T_{S3KS-S2KS}$ residuals (open circles, vertical scale on left).

than average V_S structure will slow down S3KS more than S2KS, as S3KS spends more time in the lower mantle than does the more steeply diving S2KS, along with the added affect of the raypaths being perturbed to more deeply penetrating, longer-time paths. This in turn increases $\delta T_{S3KS-S2KS}$, and similarly $\delta T_{S4KS-S3KS}$. However, owing to the closeness of the $SmKS_{234}$ raypaths, δT anomalies resulting from 1-D structures displaying lower than average D″ velocities are negligible and underpredict the observations of Fig. 4. Correcting $SmKS_{234}$ observations for long-wavelength 3-D structure using laterally homogeneous raypaths of a 1-D reference model will also underpredict the observations, as structure encountered by the separate $SmKS$ phases is negligibly different. If laterally inhomogeneous raypaths are adopted, 3-D structure will have an added effect on $SmKS_{234}$ times from raypath perturbations, and is explored in what follows. The WKM method allows construction of $SmKS$ waveforms from 2-D structures. Velocity perturbations for this method must be parametrized as a layered structure where layer thicknesses can change laterally across the structure (see Helmberger et al. (1985ab, 1995) for further discussion on the model parametrization and method). In using this technique, 2-D cross-sections through 3-D structures can be constructed and tested.

The pronounced low-velocity zone (LVZ) on the source side of the $SmKS$ paths (Fig. 5) can be parametrized for WKM input by a series of cross-sections containing various sizes and intensities of an LVZ. As a first approximation, only the source-side lower-mantle LVZ is parametrized; receiver-side structure is predicted to be small by SH12_WM13 (roughly within ±1%). The 2-D cross-sections were constructed using the PREM as a starting model, parametrized as a stack of 175 layers from the surface to the Earth's center. Thicknesses of layers in the bottom 400–900 km of the mantle were then systematically varied laterally to form large-scale LVZs. This is accomplished by thickening a given layer to extend to deeper regions, thereby displacing the velocity at a given depth by a slower value. Fig. 7 displays an example of such a model. The WKM method uses the Earth flattening approximation (e.g. see Müller, 1977), so the model is displayed as a Cartesian stack of layers. Iso-velocity contours are shown depicting the LVZ on the source side of the path; from end to end the anomaly measures about 4500 km. The center of the LVZ contains about a 2% reduction from the PREM. This model is meant to correspond to the azimuth that encounters the most anomalous structure in SH12_WM13. The structure corresponding to other azimuths can be parametrized by

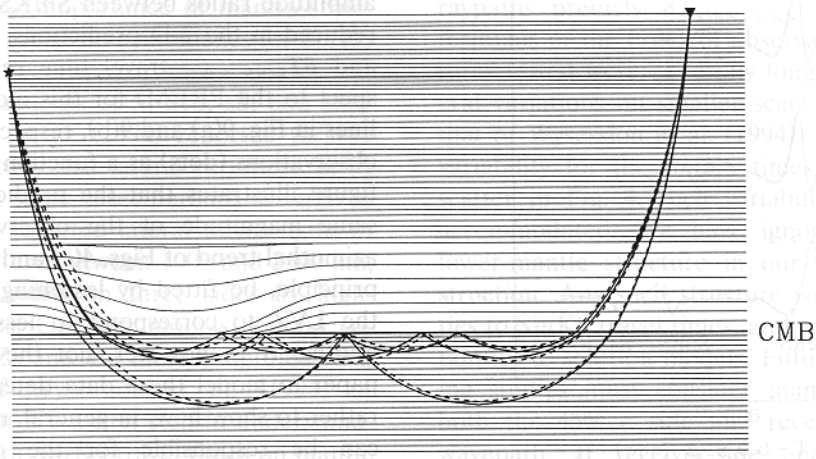

Fig. 7. Earth-flattened 2-D cross-section showing $SmKS_{234}$ first-arrival raypaths for the 2-D structure (solid) and for the PREM (dotted). Source (star) is at 500 km depth, and receiver (triangle) is at 150°.

models containing smaller sizes and intensities of an LVZ. First-arrival raypaths for $SmKS_{234}$ for the 2-D structure are shown as solid lines connecting the 500 km deep source (star) and receiver at 150° (triangle), and those for the 1-D PREM are shown as dotted lines. For this particular source–receiver arrangement, the 2-D $SmKS_{234}$ first arrival wavepaths dive more deeply to avoid the source-side lower-mantle slow anomaly. These paths are also perturbed owing to the effect of dipping velocity interfaces that compose the cosine taper LVZ. The 2-D paths of S3KS and S4KS are almost superimposed in the lower mantle (source side), which is a result of the V_S anomaly in the model. Also, owing to the source-side anomaly, 2-D receiver-side S2KS and S3KS paths are more separated than those of the PREM.

Such perturbations in raypath, as well as those in travel time owing to the reduced velocities, combine to yield $SmKS_{234}$ difference time and amplitude anomalies. Comparing WKM $SmKS_{234}$ waveforms for the model shown in Fig. 7 with those of 1-D PREM predictions illustrates such

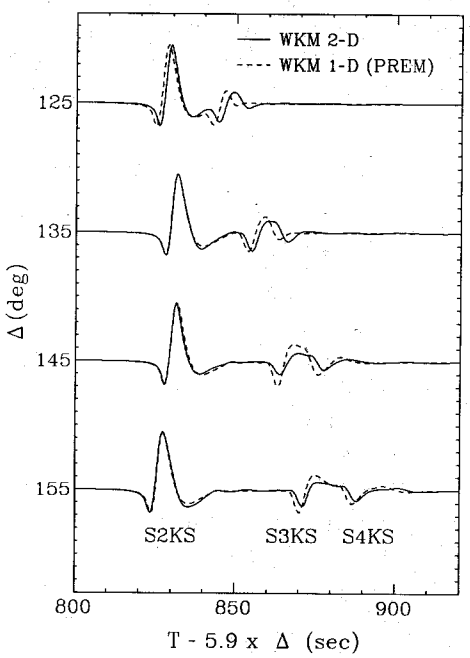

Fig. 8. WKM $SmKS_{234}$ waveform comparisons for the 2-D structure of Fig. 9 (solid) with that of the PREM (dotted).

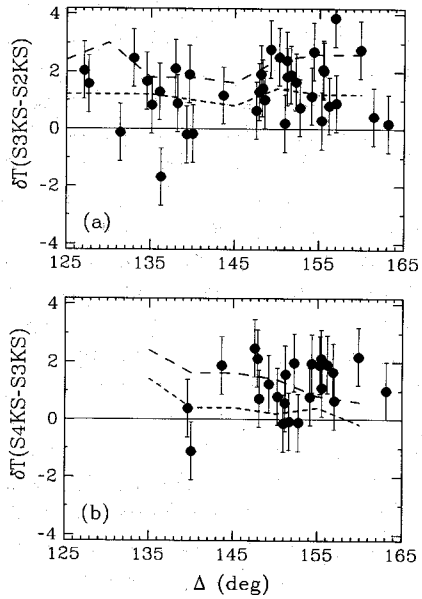

Fig. 9. (a) $\delta T_{S3KS-S2KS}$ and (b) $\delta T_{S4KS-S3KS}$ observations (solid circles) and predictions for the 2-D structure of Fig. 9 for source placement at left end of model (dotted line) and 400 km towards the anomaly from left end of model (dashed line).

travel time perturbations. Waveforms calculated from the 2-D model (Fig. 8, solid traces) exhibit larger $T_{S3KS-S2KS}$ and $T_{S4KS-S3KS}$ separations than those of the 1-D PREM (dotted traces). At closer distances (125°), absolute T_{S2KS} times are also affected by the structure. At the larger distances, amplitude ratios between $SmKS_{34}$ and S2KS are reduced in the 2-D predictions. The $\delta T_{S3KS-S2KS}$ and $\delta T_{S4KS-S3KS}$ travel time residuals (with respect to the PREM) for this model are given as lines in Fig. 9(a) and 9(b), respectively, along with observations (dots) as a function of distance. The figure illustrates that the predictions are of the same magnitude of the observations, and the azimuthal trend of Figs. 4(c) and 4(d) can thus, in principle, be fitted by lessening the intensity of the LVZ to correspond to less anomalous azimuths. It is, however, not the purpose of this paper to model these data deterministically, but rather to show how, in general, mantle structures can be responsible for the observed $SmKS$ anomalies.

Two curves are plotted in Fig. 9 with the data,

and correspond to different placements of the source location with respect to the lower-mantle LVZ. The dotted curve corresponds to the placement in Fig. 7, and the dashed curve corresponds to a source located 400 km towards the receiver from this position. The different lateral source placements in turn produce $SmKS_{234}$ raypaths that interact with different parts of the 2-D structure, resulting in different $\delta T_{S3KS-S2KS}$ and $\delta T_{S4KS-S3KS}$ residuals. The dashed curves display $\delta T_{S3KS-S2KS}$ and $\delta T_{S4KS-S3KS}$ anomalies of up to 3 s and 2 s, respectively, and range within the scatter of the observations. In moving the source 400 km closer to the LVZ, $SmKS_{34}$ waves interact more directly with the center of the anomaly than for the original source placement.

The model presented in Fig. 7 contains an LVZ with perturbations from the PREM of the order of more than 2%. Reducing the velocities more will have a greater impact on the $SmKS_{234}$ times, causing even larger difference times. Reducing the lateral scale-length of the cosine taper will also produce larger $SmKS_{234}$ difference time anomalies owing to increased raypath perturbations. For example, reducing the lateral width of the structure to 2500 km and the vertical extent of the LVZ above the CMB to 500 km results in $\delta T_{S3KS-S2KS}$ residuals up to 6 s. This is several seconds larger than observations; thus such large lateral velocity gradients may be unrealistic. Nonetheless, the 2-D wave propagation experiments illustrate the importance of mantle structure in producing travel time anomalies for SmKS waves.

In a detailed analysis of S, ScS, sS, and sScS times, Wysession et al. (1994) reported for the same region of study that lateral variations in V_S are $\pm 3\%$, and in some cases perhaps as large as $\pm 6\%$. They also reported lateral wavelengths of low-velocity structure between 1000 and 2500 km, which are surrounded on three sides by high-velocity anomalies. Our test models contain cosine tapered LVZs and are more simplified than the structure of Wysession et al. (1994) or SH12_WM13, but are a first step in understanding dependences of SmKS travel times on mantle structure. A structure such as that presented by Wysession et al. (1994) would produce more varied $\delta T_{S3KS-S2KS}$ and $\delta T_{S4KS-S3KS}$ anomalies than those predicted in Fig. 9, and whether or not this structure better fits the observations remains for future study. Rather than finding the lower-mantle model that best fits the data, our purpose here has been to show the strong effect of lower-mantle heterogeneity on SmKS times.

5. Discussion

SmKS times have been analyzed for a source–receiver geometry containing strong lowermost mantle heterogeneity. For a region in absence of such anomalies, such as that presented by Garnero et al. (1993a), $SmKS_{234}$ times are well predicted by the PREM, with the additional modification of lowering the outermost 50 km of the core V_P by 1.5%. This reduction is large enough to imply chemical stratification when using the inhomogeneity index approach of Bullen (1975). However, 1-D reflectivity method synthetic tests suggest uncertainties and non-uniqueness in structure in the outermost 25 km of the core for the LP WWSSN band pass, thus precluding confidence in such a statement.

The 2-D wave propagation experiments have demonstrated the importance of the effect of lowermost mantle heterogeneity on SmKS differential times. The combination of laterally varying structure and resulting laterally inhomogeneous raypaths predicts $\delta T_{S3KS-S2KS}$ and $\delta T_{S4KS-S3KS}$ residuals of the order of observations. The structures tested were generally long wavelength; lateral variations on smaller scale lengths (such as that of Wysession et al. (1994)) imply even more variability for the SmKS times. In viewing the scatter in Fig. 4, such variability can be easily accommodated. We have ignored receiver-side lower-mantle structure in our 2-D model construction. Any such structure will add complexities to SmKS travel times, and add further uncertainties to solution models. Future SmKS modeling studies must consider mantle structure on both the source side and receiver side of the wavepath. If receiver-side anomalies for the Tonga data can be demonstrated to contribute minimally to SmKS anomalies, then the az-

imuthal trend of the data (Fig. 4(c)) may ultimately be modeled through construction of various representative 2-D cross-sections with varying intensities and sizes of low-velocity structures using the WKM method or perhaps some 3-D method.

Complications in the S*m*KS data owing to anisotropy, as suggested by Silver and Chan (1988) for example, are not expected to play a role here, as transverse components of the LP data showed no S*m*KS energy. Slab effects (Cormier, 1989) have been assumed minimal, as only deep focus events were studied and S*m*KS waveforms were not distorted. Such complications, however, cannot be ruled out as a source of some isolated observations containing waveform anomalies. CMB topography, however, may serve to focus or defocus $SmKS_{234}$ energy, particularly the higher multiples. How topography affects $SmKS_{234}$ times and waveforms remains for future work. It is also uncertain at present how approximating 3-D lowermost mantle structure with 2-D cross-sections may neglect important 3-D focusing or defocusing and off-azimuth effects on the S*m*KS times. Such complexities, if they exist, further emphasize the importance of understanding mantle effects on S*m*KS. We have not explored D″ discontinuity structures here, which have been recently proposed to be a world-wide feature (Nataf and Houard, 1993). A 1-D D″ discontinuity structure does not significantly alter $SmKS_{234}$ times, although any 2-D D″ structure (e.g. Garnero et al., 1993c; Kendall and Shearer, 1994), such as lateral warping or thinning, may significantly affect the difference times (Helmberger et al., 1995). S-wave scattering as suggested by Haddon and Buchbinder (1987) should also complicate S*m*KS data. Utilizing $SmKS_{234}$ amplitude information in future modeling efforts may help in resolving some of the uncertainties inherent in some of these issues. Source mislocations do not alter results of our analysis, as differential travel times have been studied.

As mentioned above, previous studies have presented evidence for lower-mantle V_S lateral variations on scale lengths of O(100 km) which are smaller than the resolution of present tomographic inversion results (O(1000 km)). Such variations, especially strong lateral gradients, affect S*m*KS times and must be considered when correcting S*m*KS times for mantle structure. Otherwise, unknown mantle heterogeneity maps directly into core structure.

Garnero et al. (1988) and Garnero and Helmberger (1993) have shown how mantle structure can explain anomalous S–SKS and SKKS–SKS times for Fiji–Tonga to North America paths, which traverse a low-velocity lower-mantle anomaly beneath the southwest Pacific. Alternately, in analyzing a large data set of S, SKS, and SKKS times, Schweitzer (1990) inverted for small-scale laterally varying structure in the lower mantle with and without including the outermost 400 km of the outer core in the inversion. In that study, a heterogeneous lower mantle along with a homogenous outer core best explained the observations. Fiji–Tonga data recorded in North America, Eurasia, and Africa provide valuable and abundant data for use in S*m*KS studies. However, anomalous mantle structure must first be mapped out before these data are used to investigate variable outermost core properties.

Synthetic tests suggest that the LP data used here cannot well resolve structure in the outermost 25 km of the core. Broadband S*m*KS data for regions exhibiting little mantle heterogeneity should help in this regard. Dynamical considerations imply outer-core homogeneity (Stevenson, 1987); if the outer core departs from this it is of fundamental importance to map this and explore possible causes. For this reason, better maps of lower-mantle heterogeneity on all scales remains necessary. S*m*KS waves can supplement future inversions, following Schweitzer (1990) by inverting for 3-D mantle structure with and without permitting the outermost core to vary. Raypath inhomogeneity should be considered in such future studies.

6. Conclusions

Although outermost core heterogeneity and/or chemical stratification cannot be ruled out at present, our analysis suggests that uncertainties in lower-mantle structure preclude confident con-

clusions concerning these issues. Lower-mantle structure is shown to affect S*m*KS behavior systematically. An example of three Fiji–Tonga events is presented whereby S*m*KS paths traverse slower than average velocities in the lower mantle on the source side of the paths. WKM waveforms are synthesized for 2-D cross-sections simulating slices through the 3-D model SH12_WM13 (Su et al., 1992). Our tests indicate that such lower-mantle structure explains the size of S*m*KS anomalies observed for the Fiji–Tonga data. Mantle structure must be accurately known, or contain little heterogeneity, to allow inferences to be made on outermost core properties. If future studies indicate that regions where no lower-mantle anomalies exist consistently yield no anomalies in multi-S*m*KS paths, we will be safe in assuming that the outermost core is 1-D. With this assumption we can then use the full power of multi-S*m*KS waveform analysis to explore D″ variations.

Acknowledgments

We thank Steve Grand for useful discussions, and two anonymous reviewers for helpful comments. Lian-she Zhao helped in 2-D model parametrization. This research was supported by NSF Grant EAR-91-17781. This paper is Contribution 5374, Division of Geological and Planetary Sciences, California Institute of Technology.

References

Bloxham, J., 1990. On the consequences of strong stable stratification at the top of Earth's core. Geophys. Res. Lett., 17: 2081–2084.

Bokelmann, G.H.R. and Silver, P.G., 1993. The Caribbean anomaly: short-wavelength lateral heterogeneity in the lower mantle. Geophys. Res. Lett., 20: 1131–1134.

Bullen, K.E., 1975. The Earth's Density. Chapman and Hall, London, 420 pp.

Chapman, C.H. and Orcutt, J.A., 1985, the computation of body wave synthetic seismograms in laterally homogeneous media. Rev. Geophys., 23: 105–163.

Choy, G.L., 1977. Theoretical seismograms of core phases calculated by frequency-dependent full wave theory, and their interpretation. Geophys. J.R. Astron. Soc., 51: 275–312.

Choy, G.L. and Richards, P.G., 1975. Pulse distortion and Hilbert transformation in multiply reflected and refracted body waves. Bull. Seismol. Soc. Am., 65: 55–70.

Cormier, V.F., 1989. Slab diffraction of S waves. J. Geophys. Res., 94: 3006–3024.

Dziewonski, A.M. and Anderson, D.L., 1981. Preliminary reference Earth model (PREM). Phys. Earth Planet. Inter., 25: 297–356.

Fearn, D.R. and Loper, D.E., 1981. Compositional convection and stratification of Earth's core. Nature, 289: 393–394.

Fuchs, K. and Müller, G., 1971. Computation of synthetics seismograms with the reflectivity method and comparison with observations. Geophys. J.R. Astron. Soc., 23: 417–433.

Gaherty, J.B. and Lay, T., 1992. Investigation of laterally heterogeneous shear velocity structure in D″ beneath Eurasia. J. Geophys. Res., 97: 417–435.

Garnero, E.J. and Helmberger, D.V., 1993. Travel times of S and SKS: implications for 3-D lower mantle structure. J. Geophys. Res., 98: 8225–8241.

Garnero, E.J., Helmberger, D.V. and Engen, G., 1988. Lateral variations near the core–mantle boundary. Geophys. Res. Lett., 15: 609–612.

Garnero, E.J., Helmberger, D.V. and Grand, S.P., 1993a. Constraining outermost core velocity with S*m*KS waves. Geophys. Res. Lett., 20: 2463–2466.

Garnero, E.J., Grand, S.P. and Helmberger, D.V., 1993b. Low P-wave velocity at the base of the mantle. Geophys. Res. Lett., 20: 1843–1846.

Garnero, E.J., Helmberger, D.V. and Grand, S.P., 1993c. Preliminary evidence for a lower mantle shear wave velocity discontinuity beneath the central Pacific. Phys. Earth Planet. Inter., 79: 335–347.

Haddon, R.A.W. and Buchbinder, G.G.R., 1987. S wave scattering by 3-D heterogeneities at the base of the mantle. Geophys. Res. Lett., 14: 891–894.

Hales, A.L. and Roberts, J.L., 1971. The velocities in the outer core. Bull. Seismol. Soc. Am., 61: 1051–1059.

Helmberger, D.V., Engen, G. and Grand, S.P., 1985a. Notes on wave propagation in laterally varying structure. J. Geophys., 58: 82–91.

Helmberger, D.V., Engen, G. and Grand, S.P., 1985b. Upper-mantle cross-section from California to Greenland. J. Geophys. 58: 92–100.

Helmberger, D.V., Zhao, L.-S. and Garnero, E.J., 1995. Construction of synthetics for 2D structures; core phases. Geophys. J. Int., submitted.

Jault, D. and Le Mouël, J.L., 1991. Physical properties at the top of the core and core surface motions. Phys. Earth Planet. Inter., 68: 76–84.

Kendall, J.-M. and Shearer, P.M., 1994. Lateral variations in D″ thickness from long-period shear-wave data. J. Geophys. Res., 99: 11575–11590.

Kenneth, B.L.N. and Engdahl, E.R., 1991. Traveltimes for global earthquake location and phase identification. Geophys. J. Int., 429–465.

Kind, R. and Müller, G., 1975. Computations of SV waves in realistic Earth models. J. Geophys., 41: 149–172.

Kohler, M.D. and Tanimoto, T., 1992. One-layer global inversion for outermost core velocity. Phys. Earth Planet. Inter., 72: 173–184.

Lavely, E.M., Forsyth, D.W. and Friedemann, P., 1986. Scales of heterogeneity near the core–mantle boundary. Geophys. Res. Lett., 13: 1505–1508.

Lay, T. and Young, C.J., 1990. The stably-stratified outermost core revisited. Geophys. Res. Lett., 17: 2001–2004.

Masters, G., 1979. Observational constraints on the chemical and thermal structure of the Earth's deep interior. Geophys. J.R. Astron. Soc., 57: 507–534.

Masters, G., Bolton, H. and Shearer, P., 1992. Large-scale 3-dimensional structure of the mantle (abstract). EOS Trans. Ann. Geophys. Union, 73: 201.

Morelli, A. and Dziewonski, A.M., 1993. Body wave traveltimes and a spherically symmetric P- and S-wave velocity model. Geophys. J. Int., 112: 178–194.

Müller, G., 1977. Earth-flattening approximation for body waves derived from geometric ray theory–improvements, corrections and range of applicability. J. Geophys., 42: 429–436.

Müller, G., 1985. The reflectivity method: a tutorial. J. Geophys., 58: 153–174.

Nataf, H-C. and Houard, S., 1993. Seismic discontinuity at the top of D'', a worldwide feature? Geophys. Res. Lett., 20: 2371–2374.

Randall, M.J., 1970. SKS and seismic velocities in the outer core. Geophys. J.R. Astron. Soc., 21: 441–445.

Schweitzer, J., 1990. Untersuchung zur Geschwindigkeitsstruktur im unteren Erdmantel und im Bereich der Kern–Mantel-Grenze unterhalb des Pazifiks mit Scherwellen. Ph.D. Thesis, Frankurt University, 134 pp.

Schweitzer, J. and Müller, G. 1986. Anomalous difference traveltimes and amplitude ratios of SKS and SKKS from Tonga–Fiji events. Geophys. Res. Lett., 13: 1529–1532.

Silver, P. and Chan, W.W., 1988. Implications for continental structure and evolution from seismic anisotropy. Nature, 355: 34–89.

Silver, P. and Bina, C.R., 1993. An anomaly in the amplitude ratio of SKKS/SKS in the range 100–108° from portable teleseismic data. Geophys. Res. Lett., 20: 1135–1138.

Souriau, A. and Poupinet, G., 1990. A latitudinal pattern in the structure of the outermost liquid core, revealed by the travel times of SKKS–SKS seismic phases. Geophys. Res. Lett., 17: 2005–2007.

Souriau, A. and Poupinet, G., 1991. A study of the outermost liquid core using differential travel times of the SKS, SKKS, and S3KS phases. Phys. Earth Planet. Inter., 68: 183–199.

Stevenson, D.J., 1987. Limits on lateral density and velocity variations in the Earth's outer core. Geophys. J.R. Astron. Soc., 88: 311–319.

Su, W., Woodward, R.L. and Dziewonski, A.M., 1992. Joint inversions of travel-time and waveform data for the 3-D models of the Earth up to degree 12 (abstract). EOS Trans. Am. Geophys Union, 73: 201–202.

Su, W.-J., Woodward, R.L. and Dziewonski, A.M., 1994. Degree 12 model of shear velocity heterogeneity in the mantle. J. Geophys. Res., 99: 6945–6980.

Tanaka, S. and Hamaguchi, H., 1993. Travel times and velocities in the outer core based on the global observations of S_mKS seismic phases. Tohoku Geophys. J. (Sci. Rep. Tohoku Univ., Ser. 5), 34: 55–87.

Tanaka, S. and Hamaguchi, H., 1993c. Degree one heterogeneity at the top of the Earth's core, revealed by S_mKS travel times. In: J.-L. Le Mouel. Dynamics of Earth's Deep Interior and Earth Rotation, Geophys. Monogr. Ser., 72. Am. Geophys. Union, Washington, DC, pp. 127–134.

Tanaka, S. and Hamaguchi, H., 1993. Velocities and chemical stratification in the outermost core. J. Geomagn. Geoelectr., 45: 1287–1301.

Tanimoto, T., 1990. Long-wavelength S-wave velocity structure throughout the mantle. Geophys. J. Int., 100: 327–336.

Weber, M., 1993. P- and S-wave reflections from anomalies in the lowermost mantle. Geophys. J. Int., 115: 183–210.

Weber, M. and Davis, J.P., 1990. Evidence of a laterally inhomogeneous lower mantle structure from P- and S-waves. Geophys. J. Int., 102: 231–255.

Woodward, R.L. and Masters, G., 1991. Lower-mantle structure from ScS–S differential travel times. Nature, 352: 231–233.

Wysession, M.E., Okal, E.A. and Bina, C.R., 1992. The structure of the core–mantle boundary from diffracted waves. J. Geophys. Res., 97: 8749–8764.

Wysession, M.E., Bartko, L. and Wilson, J., 1994. Mapping the lowermost mantle using core-reflected shear waves. J. Geophys. Res., 99: 13677–13684.